Journal of Marine Science and Technology

Volume 26 | Issue 5 Article 9

SOUND AND VIBRATION ANALYSIS OF A MARINE DIESEL ENGINE VIA REVERSE ENGINEERING

Jinsiang Shaw
Institute of Mechatronic EngineeringResearch Center of Energy Conservation for New Generation of Residential,Commercial, and Industrial Sectors, National Taipei University of Technology,Taipei,Taiwan. R.O.C

Yun-Hong Wang
Institute of Mechatronic Engineering

Cherng-Yuan Lin
Department of Marine Engineering, National Taiwan Ocean University, Keelung, Taiwan, R.O.C.

Recommended Citation

Shaw, Jinsiang; Wang, Yun-Hong; and Lin, Cherng-Yuan (2018) "SOUND AND VIBRATION ANALYSIS OF A MARINE DIESEL ENGINE VIA REVERSE ENGINEERING," *Journal of Marine Science and Technology*: Vol. 26: Iss. 5, Article 9.
DOI: 10.6119/JMST.201810_26(5).0009
Available at: https://jmstt.ntou.edu.tw/journal/vol26/iss5/9

SOUND AND VIBRATION ANALYSIS OF A MARINE DIESEL ENGINE VIA REVERSE ENGINEERING

Acknowledgements

This paper is financially supported by University System of Taipei Joint Research Program under the Contract No. USTPNTUT-NTOU-106-04 and also by the “Research Center of Energy Conservation for New Generation of Residential, Commercial, and Industrial Sectors” from The Featured Areas Research Center Program within the framework of the Higher Education Sprout Project by the Ministry of Education (MOE) in Taiwan.

Journal of Marine Science and Technology, Vol. 26, No. 5, pp. 703-711 (2018)
DOI: 10.6119/JMST.201810_26(5).0009

SOUND AND VIBRATION ANALYSIS OF A MARINE DIESEL ENGINE VIA REVERSE ENGINEERING

Jinsiang Shaw[1, 2], Yun-Hong Wang[1], and Cherng-Yuan Lin[3]

Key words: finite-element analysis, biodiesel, order-tracking analysis, reverse engineering.

ABSTRACT

In this study, a sound and vibration analysis of a marine diesel engine was conducted. The vibration and sound signals of the engine under various operating conditions were measured and analyzed by applying a spectrum analysis and an order-tracking analysis. In addition, a finite-element model of the engine was constructed via reverse engineering from a 3D scan. The main causes of engine vibration and noise were clarified and identified individually through the experiments and the engine model. Finally, the biodiesel-blended diesel fuel was used for the engine for comparing sound and vibration performance with the ultra-low sulfur diesel (ULSD). In mid to high-range speeds, the biodiesel-blended diesel fuel does reduce the engine exhaust noise and vibration amplitude caused by the constant engine combustion explosion.

I. INTRODUCTION

The space inside a marine vessel is complex. There are many complex pieces of mechanical equipment or complex structures. This leads to a reverberant space. During the past few years, studies have provided detailed descriptions of noise sources, propagation paths, and signal processing (Liu, 2000; Lin, 2014; Bin, 2015). The main causes of noise are the engine power cycle, operating structure vibration, and space flow field.

The origins of vibration and noise generated by rotating machinery can be found one by one through various analytical methods. The basic method is to use fast Fourier transforms to differentiate the energy of frequency and energy size. In recent years, the time-frequency analysis adds a time variable that effectively captures the characteristics associated with the change of time. In addition, order-tracking analysis adds a speed variable that captures the speed change factor and creates order-tracking maps. In the past few years, the energy characteristics have been captured through these two analysis methods. These features effectively perform vibration and noise control (Chang, 2002; Chen and Dai, 2010; Cheng and Li, 2017; Wu et al., 2017). Therefore this study applies time-frequency analysis and order analysis to the vibration and noise analysis of marine diesel engines.

Finite-element analysis is used to simulate the sound field. Acoustic simulation is more complicated for the assumption of the environmental wall (Sie, 2014). In this study, the simulations of near-field acoustics and far-field acoustics were compared with the research results of perfect-matched layers and plane-wave radiation. This method was used to calculate far-field sound pressure levels. In addition, finite-element analysis was used to simulate the vibro-acoustics of the engine model. Past research demonstrated the influence of the size of the simulation grid. Even without using a large number of finite-element nodes, the expected results can be achieved (Masahiro et al., 2015). The engine was set up in an anechoic room for sound simulation and verification to obtain data for noise reduction improvement. The error between simulation and the actual measurement was approximately 5 dB. Therefore, a reverse engineering scan is to be used to build a model. Although the scanning model has a lower resolution than real objects, the expected research results can be achieved within the effective range.

The biodiesel was produced from vegetable lipid and mixed with the ultra-low sulfur diesel (ULSD) that can be used directly as an alternative fuel for marine diesel engines, to improve the fuel combustion efficiency and reduce fuel consumption and pollution (Lin, 2011). Biodiesel-blended diesel fuel has been verified its improvement in engine performance and air quality of the exhaust gas (Hsieh, 2014; Hsieh, 2015). In many studies, biodiesel-blended diesel fuel is shown to change the cetane number of fuel quality. That affects the noise and vibration of the engine's ignition explosion. Therefore, both biodiesel-blended diesel fuel and ultra-low sulfur diesel (ULSD) were used as the two types of diesel fuels for comparing performance in terms of engine vibration and noise levels.

Paper submitted 07/11/18; revised 08/14/18; accepted 09/10/18. Author for correspondence: Cherng-Yuan Lin (e-mail: Lin7108@ntou.edu.tw).
[1] *Institute of Mechatronic Engineering*
[2] *Research Center of Energy Conservation for New Generation of Residential, Commercial, and Industrial Sectors, National Taipei University of Technology, Taipei, Taiwan. R.O.C.*
[3] *Department of Marine Engineering, National Taiwan Ocean University, Keelung, Taiwan, R.O.C.*

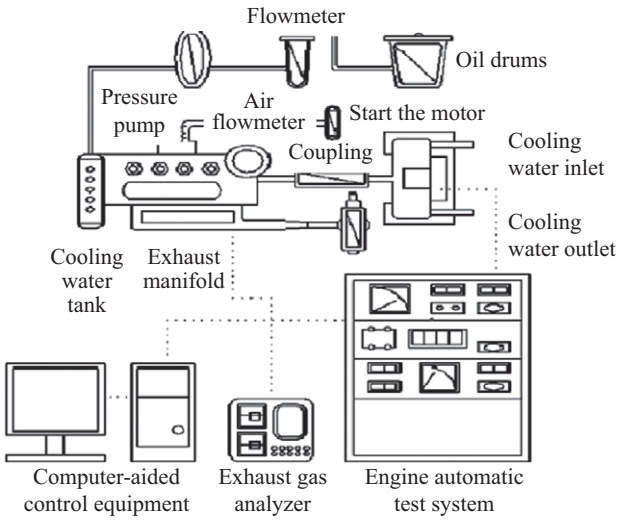

Fig. 1. Schematic diagram of the system.

II. SYSTEM DESCRIPTION

1. System Configuration

In this study, the engine model used was the ISUZU-UM4BD1, which is a marine diesel engine. Its specifications were inline four-cylinder, four-stroke, maximum output horsepower of 88 ps, cylinder bore of 102 (B) × 118 (L) mm, engine size of 1061 (L) × 720 (W) × 974 (H) mm, and body weight of 515 kg. The engine body was placed in the engine lab, along with the control computer, speed and torque control equipment, intake and exhaust tubing, flow meters, and other equipment for the experiment. Fig. 1 shows the configuration of the system setup.

2. Engine Vibration Theory

There are three main forces acting upon the engine when it operates: pressure change in the combustion chamber, reciprocating inertial force of the crankshaft-piston mechanism, and centrifugal force. All three forces produced vibration of different frequencies. An inline four-cylinder, four-stroke engine is a complex structure, not a symmetrical structure. The engine rotation movement cannot make each phase angle have the same offset forces, thus resulting in rotating imbalance. In addition, the four-stroke engine has four action strokes: intake, compression, power, and exhaust. The pressure inside the cylinder constantly changes, causing the structure to vibrate.

The mechanism inside of the engine cylinder was used to explore the internal reciprocating inertia force, rotational mass inertial force, and torsional vibration of the crankshaft. Fig. 2 is a simplified representation of a crank-and-piston mechanism. P is the instantaneous gas pressure that is a function of the angle of rotation with the crankshaft. l is the connecting rod length, and F_g is a single-cylinder gas-pressure-generated force. It is the gas pressure multiplied by the piston cross-section area. ϕ is the angle between the piston center line and the connecting rod. θ is the angle between the center line of the piston and the crank.

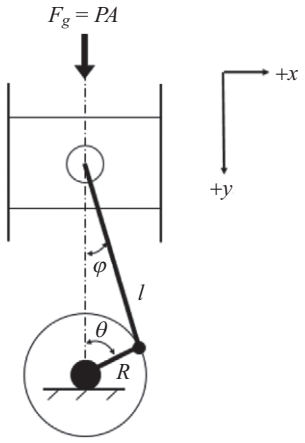

Fig. 2. Crank and piston mechanism.

Based on Fig. 2 and $R\sin\theta = l\sin\phi$, the displacement of the piston in the center line is

$$y = R(1-\cos\theta) + l\left[1-\sqrt{1-\left(\frac{R}{l}\right)^2\sin^2\theta}\right] \tag{1}$$

A general engine crankshaft radius and link length ratio is 1:4. Thus, $\left(\frac{R}{l}\right)^2\sin^2\theta = \delta$ is a small dimensionless value. Therefore $\sqrt{1-\delta} \approx \left(1-\frac{\delta}{2}\right)$ neglecting high-order terms. Eq. (1) can be rewritten as

$$y = R(1-\cos\theta) + \frac{R^2}{4l}(1-\cos 2\theta) \tag{2}$$

The velocity of the piston can be obtained by differentiating the piston displacement y by time t,

$$\dot{y} = \frac{dy}{dt} = \frac{dy}{d\theta}\cdot\frac{d\theta}{dt} = \omega\frac{dy}{d\theta} \tag{3}$$

Therefore, substituting Eq. (2) into Eq. (3) gives the velocity of piston

$$\dot{y} = R\omega\left(\sin\theta + \frac{R}{2l}\sin 2\theta\right) \tag{4}$$

Furthermore, the acceleration of the piston is

$$\ddot{y} = \frac{d\dot{y}}{dt} = \frac{d\dot{y}}{d\theta}\cdot\frac{d\theta}{dt} = \omega\frac{d\dot{y}}{d\theta} \tag{5}$$

Substituting Eq. (4) into Eq. (5) gives the acceleration of piston

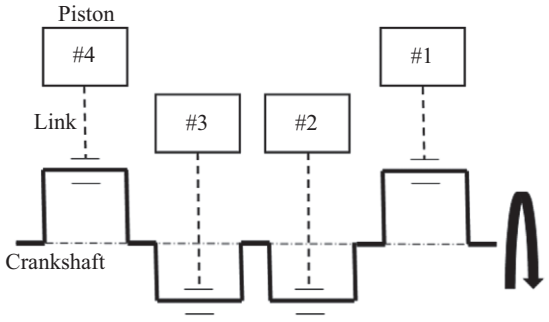

Fig. 3. Schematic diagram of the crankshaft motion.

$$\ddot{y} = R\omega^2\left(\cos\theta + \frac{R}{l}\cos 2\theta\right) \tag{6}$$

3. Engine Noise Theory

Noise in an engine room comes from many sources to form a reverberant space, including the engine burning explosion noise, structural mechanic noise, intake noise, exhaust noise, fan noise, belt noise, and air transmitted noise in space. Among these, the exhaust noise, the noise caused by the vibration of structure operation, and the noise of the space flow field are the main energy sources.

Engine exhaust noise and engine speed are related. The studied engine is a four-cylinder, four-stroke engine whose cylinder firing order is 1-3-4-2. That is, the Cylinder 1, Cylinder 3, Cylinder 4, and Cylinder 2 are sequentially ignited (see Fig. 3). However, the four stages of the four-stroke engine are intake, compression, power, and exhaust stroke. Therefore every turn of the engine produces two powers. Hence, the basic frequency of engine exhaust noise f_h (Hz) is twice the number of revolutions per second of the engine, i.e.

$$f_h = \frac{2 \cdot rpm}{60} \tag{7}$$

4. Production of the Biodiesel-Blended Diesel Fuel

This experiment used microalgal powder to extract crude oil, which was then transesterified and mixed with diesel oil to become biodiesel-blended diesel fuel. This study used Soxhlet extraction method that refluxed with organic solvents for extraction. Finally, the concentrated solvent broke down the algal cell wall, after which the oil came out of the cell. The solvent was n-hexane. This extraction method was the most efficient to have the highest crude oil extraction rate. The method heated the solvent up to 300°C, and it is much more stable than the microwave and direct-heating methods. There was up to 80% solvent recovery. The extraction time was approximately 100 min and was shorter than other extraction methods. The crude microalgal lipid was extracted and collected for a certain amount. Methanol was then added to it and heated to 60°C, which is about the boiling point of methanol. The upper liquid was removed after 10 min of heating. A triglyceride transesterification reaction with methanol of high purity occurred, i.e., fatty acid methyl ester, also known as biodiesel. For the engine test, the ultra-low sulfur diesel was added and mixed with 10 vol. % the castor-oil biodiesel to prepare the biodiesel-blended diesel fuel in this study. Table 1 compares the biodiesel produced through transesterification from microalgae with a commercial biodiesel from used cooking oil. Its combustion performance is better than that of general commercial biodiesels.

Table 1. Comparison of fuel properties of different biodiesels.

Fuel properties	Commercial biodiesel	Biodiesel from microalgae
Cetane index	52.6	55.1
Iodine value (mg I_2/g)	95.7	75.4
Kinematic viscosity (mm^2/s)	4.2	5.3

III. ENGINE REVERSE MODELING AND FINITE-ELEMENT ANALYSIS

1. Reverse-Modeling Process

Usually finite-element analysis required a complete geometric model of the system. Each feature requires a complete description to be close to reality. However, even if today's software does not use such a high-quality model, it can also achieve well-matched results in the simulation solution. In this study, a marine diesel engine was used, but its geometric model was not available. Therefore, 3D reverse modeling method for constructing the engine and engine room environment for subsequent engineering analysis is applied.

An Aniwaa handheld 3D scanner was used to construct solid model of the engine and surrounding facilities. The important features were scanned as detailed as possible. Because of the large engine room space, the environment was divided into 14 local spaces for scanning and then merged together to establish the complete model. Then, Autodesk Meshmixer software was employed for multiple overlapping, filtering scan noises, and deleting the broken surface to complete the merged model. Because the scanned file was a bitmap format (STL), it was unable to carry on the subsequent engineering analysis. The merged model had to be converted to an engineering drawing by Geomagic Design X software. This part extensively used the software's shape recognition, feature recognition, and surface recognition to convert to an engineering model. The software had a unique Live Transfer feature that could transmit complete digital model data and feature trees to quickly set up a 3D solid geometry surface model which can be seamlessly integrated with the mainstream CAD software. Finally, the engineering model was completed using PTC Creo engineering software. This model will be imported to COMSOL finite-element analysis software for engineering modal analysis.

The reverse modeling process of the engine environment is shown in Fig. 4. Note that some small wires, components, nearby

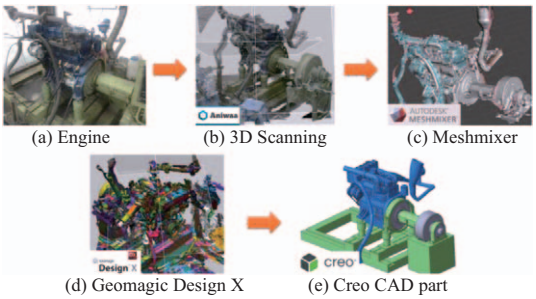

Fig. 4. Engine reverse modeling process: (a) a real engine, (b) 3D scanning, (c) merging and error correction using Meshmixer software, (d) object geometry identification using Geomagic Design X Software, and (e) Creo software CAD drawings.

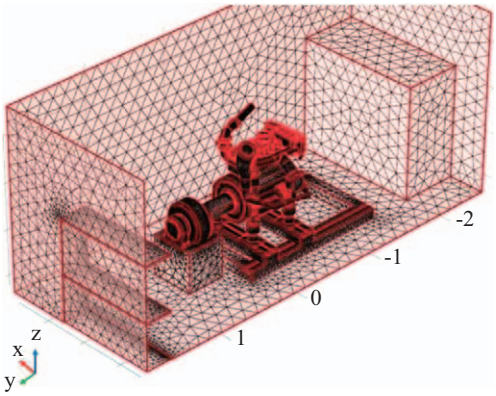

Fig. 5. Model meshing.

objects, and ceiling tubes are minor factors in the engineering analysis and thus are negligible. The scanned regions for this study include engine room walls, metal shelves, and engine-mounting brackets. The final CAD file can be imported directly to a finite-element engineering analysis software.

2. Finite-Element Model

In this study, COMSOL Multiphysics software was used for finite-element analysis of the engine. The boundary conditions include objects in the environment, the perfect matching layer, atmospheric pressure air, the engine body surface, as well as the measured vibration data. Fig. 5 shows the meshing model. A hexahedral finite element meshing yields 4,334,354 area elements, 851,828 border elements, and 112,433 side elements. After simplification, the overall model degree-of-freedom is 16,160,412. To reduce the computation time and iterations, the flexible generalized minimum residual iterative method (FGMRES) was adopted. It can solve effectively and quickly for such a large-scale acoustic model.

Finite-element analysis software COMSOL was used to simulate sound and vibration of the engine. The first method used a solid mechanics environment. The time-dependent solver was employed to obtain the engine operating conditions over time. Then, the results were used as the input to the acoustic model. The solution was obtained by vibro-acoustic analysis. This method of analysis is accurate, but the computing speed is slow, and the amount of input information is huge. Past research indicated that many physical conditions can be neglected, and reducing the finite-element quality can also give a good approximation solution. A second method is to take the actual operating conditions of the engine as the input conditions for acoustic simulation.

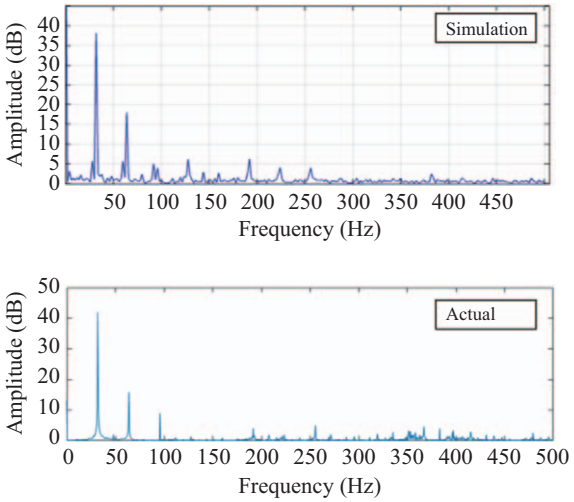

Fig. 6. Simulation and actual spectrum.

3. Sound Field Analysis

The sound propagation equation is based on the fluid flow equation. Often, the Navier-Stokes equation, a continuous momentum conservation equation, is used. When applied to solve for transient response in acoustics, it becomes Helmholtz Eq. (8). Note that Q_m is the monopoly source for each element node, ρ_c is the fluid density, P_t is the overall pressure including the pressure of the environment and the sound field changes, q_d is the dipole source, and k_{eq} is the wave number ($k_{eq} = \frac{\omega}{C}$, where ω is the angular velocity and c the sound speed). In most cases, these formulas cannot be used directly but instead solved with computer numerical algorithms. This is the reason to use COMSOL software for fast computation of these models.

$$Q_m = \nabla \cdot \left(-\frac{1}{\rho_c}\left(\nabla P_t - q_d\right)\right) - \frac{{k_{eq}}^2 P_t}{\rho_c} \tag{8}$$

According to Eq. (8) and a number of the simulation boundary conditions, including the material coefficients, the fluid environment, the structural coupling conditions, the closed space, and so on, it can be rewritten as Eq. (9), in which a_0 is the sound surface acceleration.

$$-n \cdot \left(-\frac{1}{\rho_c}\left(\nabla P_t - q_d\right)\right) = -n \cdot a_0 \tag{9}$$

Through Eq. (9), the measured vibration signal can be used

Table 2. Comparison of simulation and actual sound pressure level (dB).

RPM	Simulation	Actual	Error
650	76.3	80.76	-4.46
750	79.3	84.14	-4.84
850	83.4	92.21	-8.81
950	86.1	93.72	-7.62
1050	84.1	88.72	-4.62
1150	81.7	85.57	-3.87
1250	84.2	88.12	-3.92

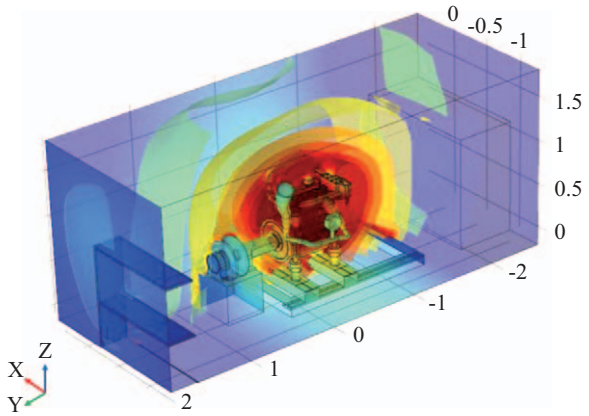

Fig. 7. Results of acoustic simulation in space.

as the input to the sound field. By using a time-dependent solution, one can obtain the transient response. Comparison of simulation results with the measured signal at a receiving point is shown in Fig. 6. Consequently through this method, the acoustic sound field in the space can be simulated. As shown in Fig. 7, the generated sound pressure level and the sound frequency in the engine room can be clearly observed.

Table 2 lists the simulated and actual sound pressure levels at the same measurement point. It is located 2 m in front of the engine and 1 m above from the ground. Simulated engine noise data were obtained from the vibration of the engine operation. This method does not include the sound of the engine ignition explosion. Hence the simulated results were 4 to 5 dB lower than the actual values. It is noted that there were amplitude peaks around 950 RPM both in simulation and experiment results, which in fact came from the resonance noise of the building. This amplitude peak disappeared in simulation if the building boundary condition was not used in the simulation model (namely, with perfect matched layer as the boundary condition). The dimensions of the building of the engine test room are 628 cm in length, 314 cm in width, and 276 cm in height.

In addition, this study also used the frequency domain analysis to solve the acoustical environment in the engine laboratory. Namely, a huge impulsive sound source is employed to excite the space. It allows the sonic energy in the space to propagate, reflect, rebound, and weaken. This spectrum analysis can obtain the frequencies that concentrate energy in the space, and its position can be analyzed. After that, the acoustic spectrum of every point in this model is plotted, as shown in Fig. 8. That is, every color represents a frequency response plot of each element node. For example, the purple peak is a resonant frequency at 153 Hz measured near the iron cabinet in this room. These frequency peaks were verified with actual measurements in the spectrum analysis and time-frequency analysis.

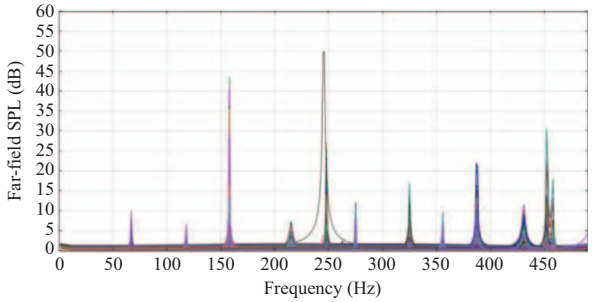

Fig. 8. Frequency response diagram.

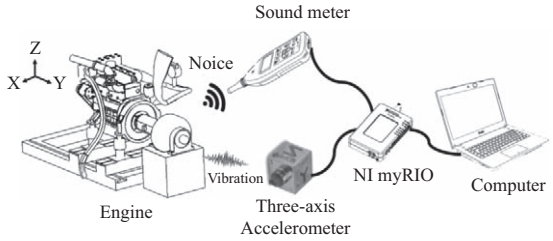

Fig. 9. Engine sound and vibration measurements.

IV. TIME-FREQUENCY AND ORDER ANALYSIS

1. Experimental Setup

In this study, the dynamic properties of engine vibration were captured using a three-axis accelerometer. In the meantime, the engine noise was collected by a sound level meter. These two signals were obtained by the NI myRIO processor featuring FPGA high-frequency module. In this way, real-time signal analysis of sound and vibration could be performed on the computer with the LabVIEW software, as shown in Fig. 9.

In this study, a PCB-356A31 three-axis accelerometer was used. The measuring position was on the surface of the engine head. For the case when the engine was running at a fixed idle speed of 650 RPM, the vibration analysis was shown in Fig. 10, which was in the x-direction with the largest vibration amplitude. In the figure the upper part is the frequency domain, and the lower part is the time domain. The first and second major vibration energies were concentrated at 10.83 Hz and 21.66 Hz, respectively. These are predicted as $\cos\theta$ and $\cos 2\theta$ terms in Eq. (6) because an engine speed of 650 RPM corresponds to 10.83 RPS (Hz), the fundamental driving frequency of the engine crankshaft.

In the acoustic analysis, an NL-20 sound level meter was used.

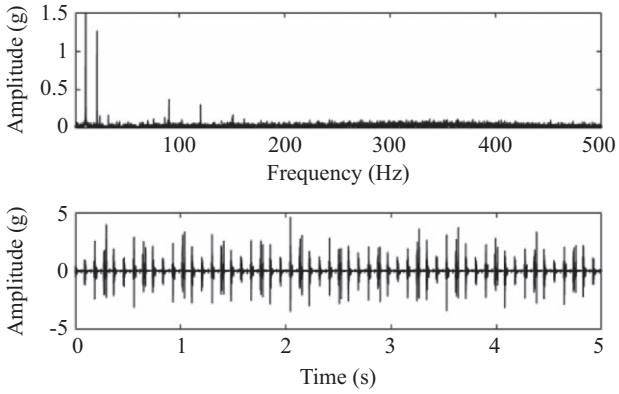

Fig. 10. Vibration analysis at engine idle speed of 650 RPM.

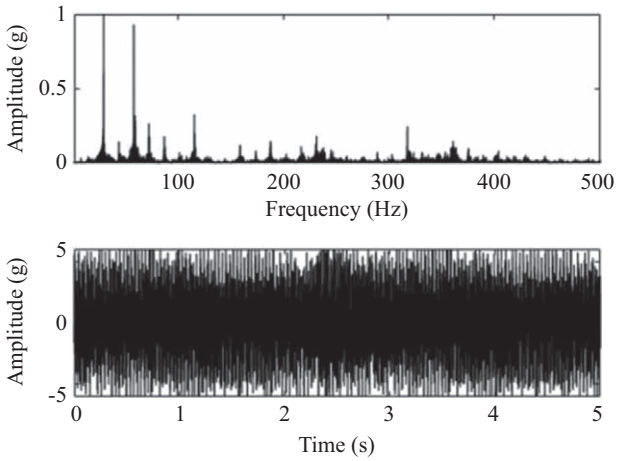

Fig. 11. Acoustic analysis at engine speed of 950 RPM.

Its effective measuring frequency range was 20 to 8000 Hz. The measurement point was 2 m from the front of the engine and 1 m above the ground floor. For example, when the engine was fixed at a speed of 950 RPM, the sound analysis was shown in Fig. 11. The first frequency peak was at 31.67 Hz, the fundamental tone of the engine exhaust noise. The engine exhaust noise can be verified by Eq. (7) with frequency twice the number of revolutions per second of the engine. In addition, the second-highest peak at 63.33 Hz was the second harmonic of the exhaust noise. There were also high energies at higher frequencies, which will be verified in the acoustic finite-element analysis.

By comparing the spectrum of vibration and noise analysis, it can be found that the main energies are concentrated in the low-frequency area. The engine speed used in this study was only from 650 to 1250 RPM (10.83 to 20.83 Hz). Though the sound meter only measured noise with frequency above 20 Hz, it still could be employed to detect engine noises and related harmonic peaks

2. Time-Frequency Analysis

An engine is a complex body and runs at varying speeds.

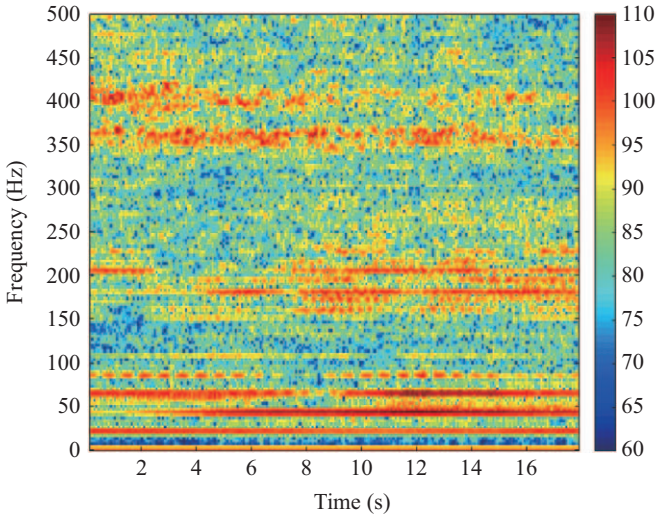

Fig. 12. Engine noise time–frequency chart.

The study in the previous sections revealed that many noise and vibration energies depend on time change. Consequently, time-frequency analysis will be employed to capture time-varying factors. The noise is a sonic energy in the air. It can spread and rebound with objects and the surrounding walls in the space. In the previous section, finite-element analysis was used to analyze the environmental acoustics. In this section, the first example is to measure the engine noise with a constant engine speed by surrounding it in one turn, and the noise distribution in the time-frequency chart is shown in Fig. 12 where the time axis corresponds to different location around the engine. Recorded noises have different energy frequencies and some of them similar to those as predicted in Fig. 8. Note also that most of the frequency peaks have different intensities at different locations. However, engine noise has different frequency feature for each rotation speed. The main energy frequencies are the crankshaft vibration and engine exhaust noise that depend on the rotation speed. Therefore, a varying speed analysis was included. The engine speed was increased from idle speed 650 RPM to the highest speed of 1250 RPM, and the resulting time-frequency noise and vibration analysis were shown in Fig. 13 and Fig. 14, respectively. In Fig. 13 two noises with high sound pressure level are clearly seen with two times and four times the rotational speed; they are the engine exhaust noise and its harmonics. Moreover, looking at a higher frequency region, there were some feature energies depending on the rotation speed. It may be caused by the gearbox of the engine output shaft. This can be verified by a vibration analysis collected by the accelerometer. In Fig. 14 the first and second time-dependent energy frequencies were due to vibrations of the engine crankshaft, where frequencies were at 1- and 2-times the rotation speed. In the next section, order analysis is applied for the speed-dependent feature energies.

3. Order Analysis

In the previous sections, we found that major components

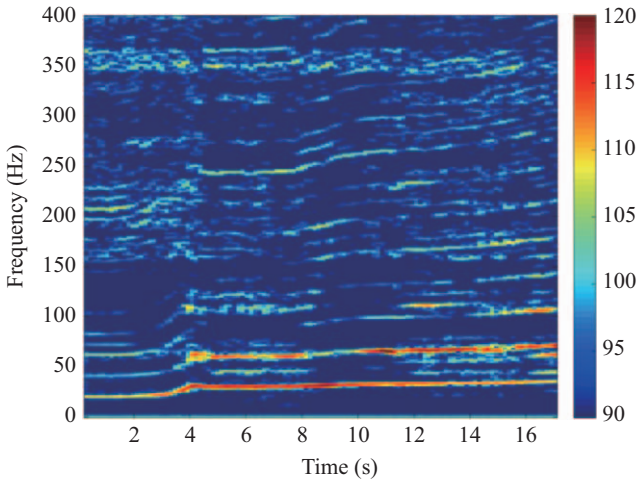

Fig. 13. Noise time-frequency chart with varying speeds.

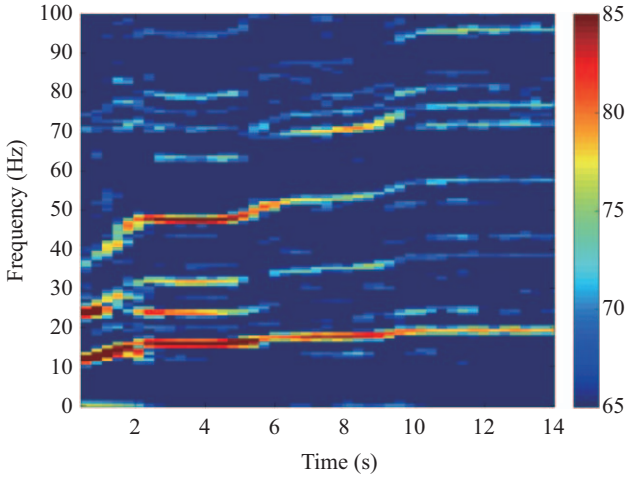

Fig. 14. Vibration time–frequency chart with varying speeds.

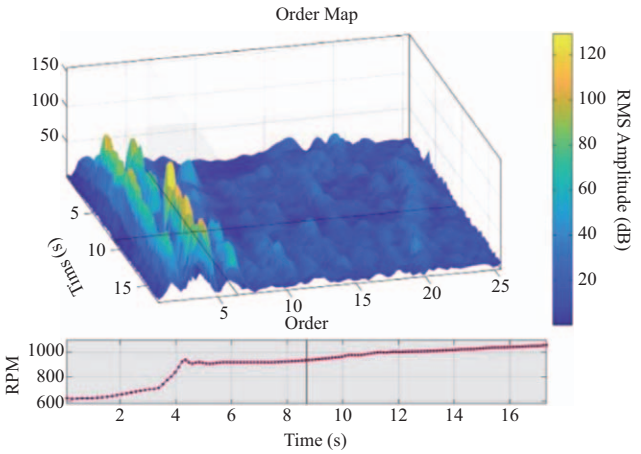

Fig. 15. Noise order map.

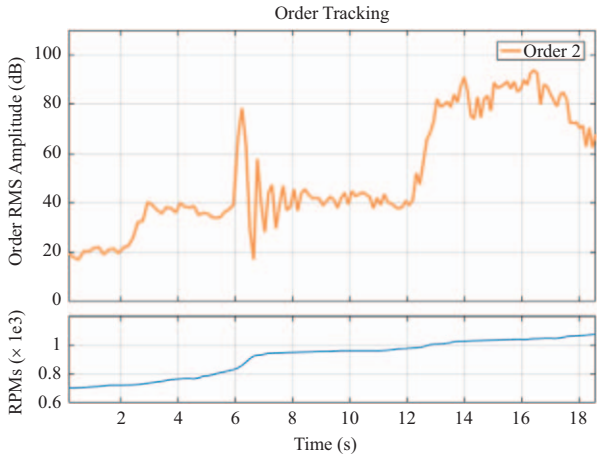

Fig. 16. Noise Order 2 tracking analysis (ULSD).

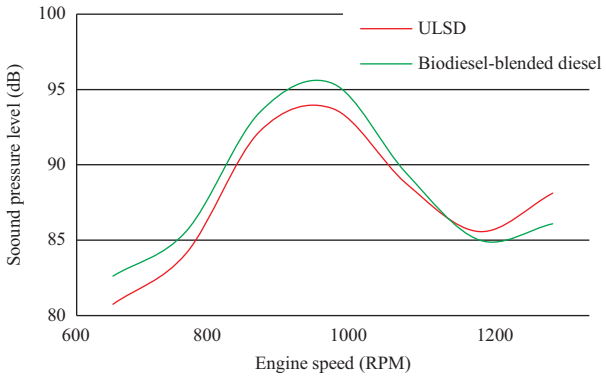

Fig. 17. Comparison of sound pressure levels using two different fuels.

of vibration and noise are related to the rotational engine speeds. Hence, order analysis is employed to identify and isolate these speed-related sound and vibration components. The noise order map is shown in Fig. 15, where the lower plot indicates that the engine speed increases with time from the idle speed 650 RPM to the highest speed of 1250 RPM. As shown in Fig. 15, the main source of noise comes from Order 2 and Order 4, and other energy orders are much smaller. Order 2 noise is the engine exhaust noise, because there are two exhausts per revolution, and Order 4 noise is just the harmonics of Order 2. The amplitude of Order 2 noise as rotational speed increases is shown in Fig. 16, where an upward trend of noise amplitude is observed until the speed exceeds a certain limit and the noise amplitude starts to fall down thereafter to reach steady state. Another point to be noticed is the sharp oscillation of noise amplitude beginning at the sixth second between speeds of 900 and 950 RPM. This is caused by the acoustic resonance of the laboratory space; hence, there is a large energy peak in the sixth second.

In this study, the biodiesel-blended diesel fuel and ultra-low sulfur diesel (ULSD) were used for the engine performance comparison in terms of noise and vibration amplitudes. According to the above sections, the main engine vibration energy comes from crankshaft operation, and the main energy of noise comes from the exhaust noise. The performance comparison is based on the amplitude of the vibration and the sound pressure level of the noise. Fig. 17 illustrated sound pressure level compa-

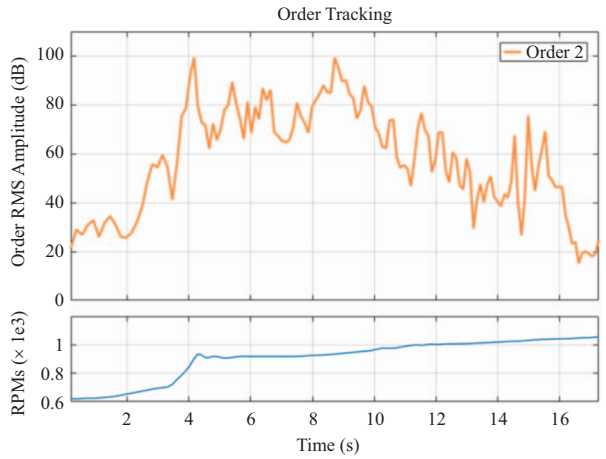

Fig. 18. Noise Order 2 tracking analysis (biodiesel-blended diesel fuel).

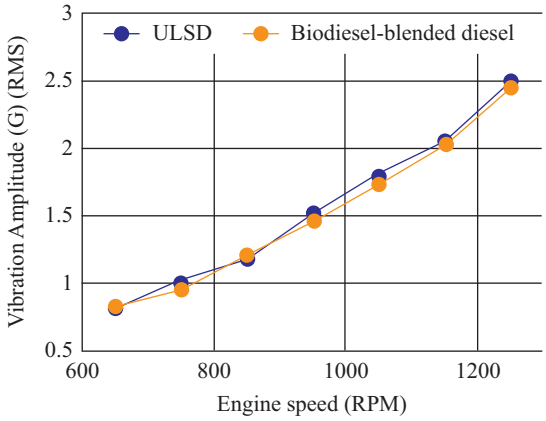

Fig. 19. Comparison of vibration amplitude using two different fuels.

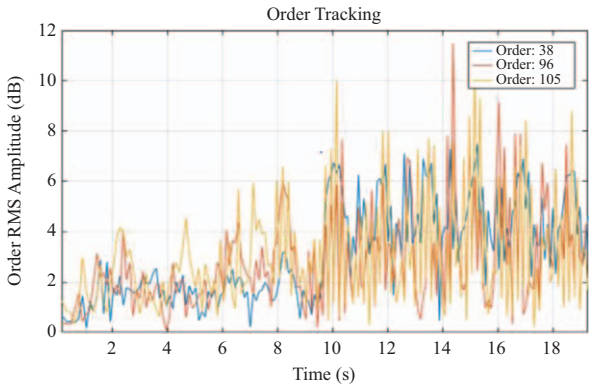

Fig. 20. Vibration order tracking using ULSD.

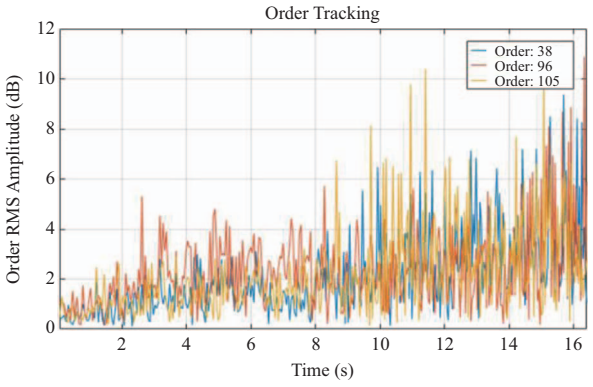

Fig. 21. Vibration order tracking using biodiesel-blended diesel fuel.

rison for the use of the biodiesel-blended diesel fuel and ultra-low sulfur diesel (ULSD), from the idle 650 RPM up to 1250 RPM. There is a crossover frequency at about 1100 RPM; below it the biodiesel-blended diesel fuel having larger sound pressure level than the ultra-low sulfur diesel; above it the biodiesel-blended diesel fuel outperforming the ultra-low sulfur diesel. Note that the biggest sound occurs at around 900 RPM for both fuels due to acoustic resonance of the laboratory space. At present, the maximum speed of the engine under empty load can only reach 1250 RPM. Therefore using the biodiesel-blended diesel fuel can improve the noise quality of the engine at high operation speeds.

Next, the order tracking method was used to analyze the engine exhaust noise energy (recall that Order 2 noise is the engine exhaust noise), as shown in Fig. 16 (for the ultra-low sulfur diesel) and Fig. 18 (for the biodiesel-blended diesel fuel). It was observed again that the biodiesel-blended diesel fuel produced a higher exhaust noise than the ultra-low sulfur diesel when the engine speed was low. However, there also appeared to crossover at high frequency. This verified not only the engine noise was mainly due to the exhaust noise, but also that the improvement of the fuel quality using the biodiesel-blended diesel fuel can reduce engine noise as well at high speeds.

As for the comparison in vibration amplitudes for two different diesels, the result was shown in Fig. 19. The use of the biodiesel-blended diesel fuel slightly reduced the vibrational energy; only at high speeds it was more obvious. This is because the main vibration energy comes from crankshaft rotation and its harmonics, which had little to do with the fuel used. However, the biodiesel-blended diesel fuel did improve the fuel burning explosion performance in the cylinders during power stroke. Li et al. (2016) measured the pressure changes inside the engine cylinder. The vibration in the combustion chamber of the engine came from the combustion explosion and the piston. The feature frequency of the combustion explosion was 4 to 12 kHz, and the feature frequency of piston impact was 1 to 3 kHz. In the time-frequency analysis in this study, there were also relevant frequencies in high-frequency areas. However, the burning energy was not concentrated so that the feature frequency cannot be accurately captured. Time-frequency analysis just showed the energy spread in high-frequency areas that were found in broadband. Therefore, the order-tracking method was used here to extract the orders with higher energy in the high-frequency region. This study selected three higher Orders of 38, 96, and 105 distributed at 1 to 3 kHz.

The high-order-tracking map in vibration for the ULSD and biodiesel-blended diesel fuel were shown in Figs. 20 and 21,

Table 3. Comparison of the RMS amplitude.

Order number	ULSD	Biodiesel-blended diesel
38	3.7881	2.6937
96	3.8071	2.8117
105	3.4112	2.8259

respectively. The data in both figures were obtained using various speeds from 650 RPM to 1250 RPM. In Fig. 20, it increased to 1000 RPM in approximately 10 s, while in Fig. 21, it rose to 1000 RPM in approximately 23 s. In the previous analysis of the noise order map, the biodiesel-blended diesel fuel has a smaller sound pressure level at high rotating speeds. Likewise, the vibration order analysis also verified that the vibration amplitudes for the biodiesel-blended diesel fuel at high rotating speeds were smaller than those for the ultra-low sulfur diesel. The RMS amplitude comparison of vibration was shown in Table 3. Hence the use of the biodiesel-blended diesel fuel improved both the noise and vibration at high engine operation speeds.

V. CONCLUSION

Different sources of diesel engine vibration and noise were accurately captured and identified through time-frequency and order-tracking analysis in this paper. Engine vibrations primarily originate from the crankshaft, piston strike, and fuel combustion explosions. The sounds primarily originate from the engine exhaust gas and its interaction with the engine room, which spreads and rebounds in space. This causes high-energy sounds at specific frequencies. In addition, finite-element analysis of the system model from reverse engineering using 3D scans of the engine can help identify the feature frequencies of the engine and spatial sounds inherent in the environment. Finally, the biodiesel-blended diesel fuel and ultra-low sulfur diesel were compared in terms of engine noise and vibration performance. The biodiesel-blended diesel fuel reduced the engine exhaust noise and vibration at the high-speed range.

ACKNOWLEDGEMENTS

This paper is financially supported by University System of Taipei Joint Research Program under the Contract No. USTP-NTUT-NTOU-106-04 and also by the "Research Center of Energy Conservation for New Generation of Residential, Commercial, and Industrial Sectors" from The Featured Areas Research Center Program within the framework of the Higher Education Sprout Project by the Ministry of Education (MOE) in Taiwan.

REFERENCES

Bin, H. L. H. (2015). Research of noise and vibration analysis for structures involving transfer path and sound source. Ph.D. Thesis, Graduate School of Science and Engineering, Doshisha University, Japan.

Chang, J. R. (2002). Application of vibration and noise signals to fault detection of engine. Master Thesis, Department of Vehicle Engineering, National Taipei University of Technology, Taiwan, Republic of China. (in Chinese)

Chen, A. Y. and X. L. Dai (2010). Internal Combustion Engine Vibration Analysis with Short-term Fourier-transform. Proceeding of International Congress on Image and Signal Processing, 4088-4091.

Cheng, J. and S. R. Li (2017). IC engine vibration time-frequency analysis based on a novel fast matching pursuit algorithm. Proceeding of IEEE 2nd Advanced Information Technology, Electronic and Automation Control Conference (IAEAC), Chongqing, China, 2227-2230

Hsieh, W. S. (2014). The study on the diesel engine performance of using different nano Al2O3 in high density emulsion fuel. Master Thesis, Department of Marine Engineering, National Taiwan Ocean University, Taiwan, Republic of China. (in Chinese)

Hsieh, Y. C. (2015). Fuel characteristics of microalgae biodiesel produced through in situ transesterification. Master Thesis, Department of Marine Engineering, National Taiwan Ocean University, Taiwan, Republic of China. (in Chinese).

Li, G. X., F. S. Gu, N. Wei, Y. D. Xu and A. Ball. (2016). A validated finite element model for predicting dynamic responses of cylinder liners in an IC engine. Proceedings of 22nd International Conference on Automation and Computing (ICAC), Colchester, UK 126-131.

Lin, B. Y. (2011). Investigation on lipid extraction of microalgae assisted by microwave and ultrasound. Master Thesis, Department of Marine Engineering, National Taiwan Ocean University, Taiwan, Republic of China. (in Chinese)

Lin, L. M. (2014). The study of engine-room structural vibration and noise coupling of merchant vessel - a case study of 1,800 T.E.U. container ship. Master Thesis, Graduate Institute of Manufacturing Technology, National Taipei University of Technology, Taiwan, Republic of China. (in Chinese)

Liu, S. Y. (2000). The investigation of the noise estimation in ship compartment. Master Thesis, Department of Engineering Science and Ocean Engineering, National Taiwan University, Taiwan, Republic of China. (in Chinese)

Masahiro, A., T. Nobutaka and A. Ito (2015). Transfer path analysis and construction of sound source model using inverse-numerical acoustic analysis. Journal of the Japanese Society of Agricultural Machinery and Food Engineers 77(3), 186-196.

Sie, M. T. (2014). Study on the variations of sound pressure of loudspeaker system from the geometry of interior box. Master Thesis, Master's Program of Electro-Acoustics, Feng Chia University, Taiwan, Republic of China. (in Chinese)

Wu, Q. J., W. Zhang, S. M. Li, Y. Xin and Y. Xin (2017). Order analysis of diesel engine in accelerating stage based on Vold-Kalman method. Proceeding of 2nd International Conference on Robotics and Automation Engineering, Shanghai, China, 306-310.